Geoderma 468 (2026) 117772

Contents lists available at ScienceDirect

Geoderma

journal homepage: www.elsevier.com/locate/geoderma

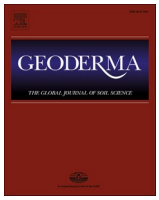

The role of weathering and aeolian inputs on clay minerals and geochemistry in Podzols on ophiolitic materials

Michele E. D'Amico [a,*], E. Bonifacio [b], A. Cavallo [c], M. Egli [d], F. Previtali [c]

[a] DISAA, University of Milano, Via Celoria 2, 20133 Milano, Italy
[b] DISAFA, University of Torino, Largo Braccini 2, 10095 Grugliasco, TO, Italy
[c] DISAT, University of Milano Bicocca, Piazza della Scienza 1, 20124 Milano, Italy
[d] Department of Geography, Winterthurerstrasse 190, 8057 Zürich, Switzerland

ARTICLE INFO

Handling Editor: Dr Karen Vancampenhout

Keywords:
Alpine soils
Mass balance calculation
Serpentinite
Saharan dust

ABSTRACT

The process of podzolization in soils developed from ultramafic materials remains enigmatic, despite a few isolated cases described in subalpine areas under particularly acidifying vegetation and wet microclimatic conditions. The aim of this study was to elucidate the pedogenic processes operating in Podzols developed under humid subalpine vegetation on ultramafic and mafic parent materials in the northwestern Alps. We used clay mineralogical and geochemical approaches, also accounting for the possible contribution of aeolian inputs. The results indicate that weathering was particularly intense under these subalpine conditions, driven by strong soil acidification and resulting in extensive dissolution of serpentine minerals and in the transformation of primary Mg-chlorite into Al- and Fe-rich smectites and vermiculites, via intermediate Fe-rich soil chlorites and hydroxy-interlayered minerals. Mass balance calculations and chemical weathering indices consistently indicate a high degree of weathering and substantial elemental losses associated with podzolization in these subalpine soils. During pedogenesis, up to ~ 80% of Mg and Si, ~85% of Ni, and ~ 65% of Cr appear to have been removed from the soil profiles.

However, weathering of ophiolitic parent rocks alone cannot fully account for the observed soil geochemistry. Aeolian inputs—primarily Saharan dust and possibly minor contributions from late-glacial loess—are required to explain the elevated contents of relatively immobile elements, particularly Al, Fe, Zr, and Ti, and these exogenous materials likely also influenced the mineralogical composition of the fine soil fractions. These results highlight the combined role of intense chemical weathering and external material inputs in the development of Podzols on ultramafic substrates under favorable climatic and ecological conditions.

1. Introduction

Chemical weathering, clay mineral formation and pedogenesis on ultramafic materials have been intensively studied in many tropical regions, mostly because of the economic interest in metal-rich lateritic soils (e.g., Nahon et al., 1988, Garnier et al., 2009). In temperate environments, the number of studies is small, and even smaller in boreal or subalpine habitats (e.g. Bulmer and Lavkulich, 1994; Lessovaia et al., 2016a,b). However, the interest in serpentinite weathering is high, as soils formed from ultramafic materials are particularly rich in heavy metals and are potentially a source of contamination for surface waters and crops. Furthermore, the products of ultramafic weathering vary with climate and with additional, more specific pedogenic processes, such as e.g. podzolization. Knowing the development traits of clay minerals helps understanding metal mobility, potential bioavailability and potential ecotoxicological risks (e.g. Caillaud et al., 2009).

Ultramafic rocks are chemically simple: Si, Mg, and Fe (as oxides) account for 80–90% of the average composition while Al_2O_3 and CaO are below 1.8% and 0.8%, respectively. However, in temperate climates, a large variety of clay minerals has been detected in soils formed from these relatively simple rocks, depending on age and site conditions. The weathering products are influenced by drainage and topography: well-drained upper slopes favor vermiculite, whereas smectites dominate under less leaching-dominated conditions (Bonifacio et al., 1997). In humid soils, neoformed smectite is thought to be the dominant weathering product of serpentine (Rabenhorst et al., 1982, Bonifacio et al.,

* Corresponding author.
E-mail address: michele.damico@unimi.it (M.E. D'Amico).

https://doi.org/10.1016/j.geoderma.2026.117772
Received 15 October 2025; Received in revised form 24 December 2025; Accepted 9 March 2026

1997), derived from the interaction of antigorite dissolution and Mg- and Al-rich chlorites, to form soil chlorite and Fe-rich smectites, with the addition of Fe oxy-hydroxides and the release of Mg^{2+} into solution (Ducloux et al., 1976). Thermodynamic modeling indicated that Fe(III)-Al hydroxide would be more stable than Mg-hydroxides (in a neutral pH range), suggesting that nontronite (Fe-rich smectite) is more stable than saponite (Mg-rich smectite). The latter is stable at high pH values and humidity (Senkayi et al., 1981). Despite its frequent occurrence, smectite formation from serpentine weathering remains enigmatic (Bulmer, 1992), because of its high structural Al content that stands in contrast to the low content of Al in the parent material.

In temperate settings, chlorite is often the only Al-bearing mineral in the parent material, derived from chlorite-schist lenses within serpentinite bodies (Caillaud et al., 2004, 2006). Therefore, the neoformation and development of clay minerals will depend exclusively on Al derived from it. Fe and Al contents are usually the highest in surface horizons (because of residual accumulation caused by Mg and Si leaching), and the clay minerals will be rich in Fe and Al (Fe-rich smectites and kaolinite).

Similar weathering patterns occur in boreal and subalpine soils, and podzolization has been reported on mafic (Lessovaia et al., 2016b) and ultramafic materials (D'Amico et al., 2008), affecting metal dynamics and clay mineral formation. If podzolization is active, the mobility of Al, Fe and potentially toxic elements is enhanced (e.g. Räisänen et al., 1997; D'Amico et al., 2009; Kowalska et al., 2021), even though a part of them might then be fixed within spodic horizons. Whichever the pedogenic process, the serpentine mineral content increases with depth because of its high weatherability under atmospheric conditions, showing an opposite trend to that of quartz (Sasaki et al., 1968). This latter accumulates residually during ultramafic weathering and its concentration increases with respect to the low contents typical of the parent material, particularly in surface horizons. Several clay minerals appear in the most weathered horizons, such as vermiculite (derived from chlorite weathering in E horizons, according to Sasaki et al., 1968), or hydroxy-interlayered smectites (HIS) and vermiculites (HIV), chlorite, talc and serpentine (in the Bs1 horizon of a cemented Podzol (Bulmer and Lavkulich, 1994). Often, clay mineralogy indicates a low soil development degree: for example, Bulmer et al. (1992) found chlorites, serpentine, talc, and only traces of smectites in the finest fraction of ultramafic B horizons covered by sialic tephra. In similar Bw-Bs horizons in Switzerland, serpentine was the most abundant mineral, with a minor contribution of kaolinite, illite, soil chlorites and quartz (Gasser et al., 1994), evidencing aeolian inputs.

Bulmer (1992), in a review about the weathering of ultramafic rocks, showed how at low pH values serpentine minerals tend to dissolve: these minerals are stable only in a small range of high pH values and with high Mg^{2+} concentrations in the soil solution (Lindsay, 1979). Hydroxy-interlayered minerals form from the weathering of chlorites, while serpentine mostly dissolves.

Many of the previously cited references indicate implicitly or explicitly that aeolian addition of some components (e.g. Al, quartz in the surface horizons) seems necessary to allow such a weathering pathway in serpentine soils. Although aeolian silt may inhibit podzolization in some environments (e.g. Musielok et al., 2022), Holocene aeolian inputs are necessary to explain the geochemical composition of Podzols developed on specific parent materials. Examples include Podzols formed on Late Pleistocene aeolian quartz sands in NW Europe (van Mourik and de Vet, 2015) and on quartz-rich residua from dolostone dissolution (D'Amico et al., 2023), highlighting the widespread influence of aeolian deposition on pedogenesis.

Accordingly, this study aims to test the following hypotheses: a – serpentine mineral dissolution and chlorite weathering pathways characterize podzolic soils developed on ultramafic materials; b – trace elements are mobilized and leached thanks to the podzolization process; and c – aeolian inputs play a significant role in controlling the geochemistry of these podzolic soils developed on atypical parent materials.

To address these objectives, we investigated three subalpine soil profiles developed on serpentinite and mafic rocks in the Western Italian Alps, chosen from previous studies that have evinced the occurrence of podzolization processes (D'Amico et al. 2008, 2009).

2. Materials and methods

2.1. Study area

Three soil profiles (Fig. 1) were described in the Chalamy Valley inside Mont Avic Natural Park, a protected ophiolitic area in the Valle d'Aosta Region, NW Alps. They were chosen among six previously studied and described soils, corresponding to P2, P4 and P6 in D'Amico et al. (2008; 2009, Fig. 1). P2 is classified as Albic Ortsteinic Podzol (Loamic), P4 and P6 are respectively Hyperdystric Endoskeletic Cambisol (Loamic, Protospodic) and Hyperdystric Cambisol (Loamic, Protospodic). In all three profiles podzolization is an active pedogenic process. They were under a subalpine *Pinus uncinata* M. and *Larix decidua* L. forest with understory dominated by *Rhododendron ferrugineum* L. and other Ericaceae. The elevation is between 1830 and 2117 m a.s.l., and the slope was exposed to the North; the average yearly temperature is between 2°C and 3°C (Mercalli and Cat Berro, 2003), and average precipitation is around 1000 mm (data derived from the nearby weather stations located in Praz Oursie, 840 mm y^{-1}, and in Pontboset, 1260 mm y^{-1}, to the south, ARPA VDA). Snow cover normally lasts from early November to late May. The Chalamy Valley is totally carved into ophiolitic rocks, with serpentinite (of antigoritic type) being the most common lithology (Dal Piaz et al., 2011). Associated with serpentinite there are many 1–5 m thick chlorite-schist and talc-schist lenses, as well as metagabbro and amphibolite outcrops in small, separated areas. Local Pleistocene glaciers actively mixed the different ophiolitic clasts and therefore the parent material of the three soils is glacial till composed of ultramafic (serpentinite and chlorite-schist) and mafic rocks (gabbros and amphibolites) in different proportions (Table 1). P2 had a parent material dominated by mafic rocks (ca. 90%), while P4 and P6 were dominated by serpentinite, with only traces of mafic materials. The Chalamy Valley was probably free from glacial ice after the LGM (between 22 and 15 ka BP), as shown by pollen records in a peat bog located not far from P6 and P4 (Arobba et al., 2016). The full characterization of the soil profiles is reported elsewhere (D'Amico et al., 2008) but the main chemical properties of the soils are shown in Table S1.

2.2. Field sampling and laboratory methods

The bulk density (BD) of the fine earth (< 2 mm) was measured by sampling 2–3 cylinders (100 cm^3) from each genetic horizon, after subtraction of the volume and the weight of the stone fragments.

The mineralogy of the clay fraction was analysed by X-Ray Diffraction (XRD) on oriented samples, with a Diffractometer X'Pert PRO, Cu radiation from 2° to 15°2θ (steps of 0.02°2θ, 1 s/step). Clay minerals were identified by comparing peak position, intensity and shape in the XRD patterns obtained after several pre-treatments according to Thorez (1975), while the identification of accessory minerals was made following the peak positions reported by Brown (1980). Clays were separated via centrifugation, after destruction of organic matter with diluted H_2O_2, and removal of Fe-oxides with Na-dithionite-citrate-bicarbonate (DCB). After separation, the clay fraction was saturated with $MgCl_2$ and then washed until the excess $MgCl_2$ was removed. After the XRD analysis on air-dried samples, the Mg-saturated clays were solvated using ethylene–glycol (EG) and analysed to detect the presence of smectites (partial shift of the 1.4 nm peak towards 1.6–1.7 nm) or smectite-vermiculite/chlorite mixed layers (partial shift of the 1.4 nm peak towards 1.5–1.6 nm), or smectite-illite (partial shift of the 1.0 nm peak towards 1.2–1.3 nm).

Another aliquot of the clay fraction was saturated with KCl,

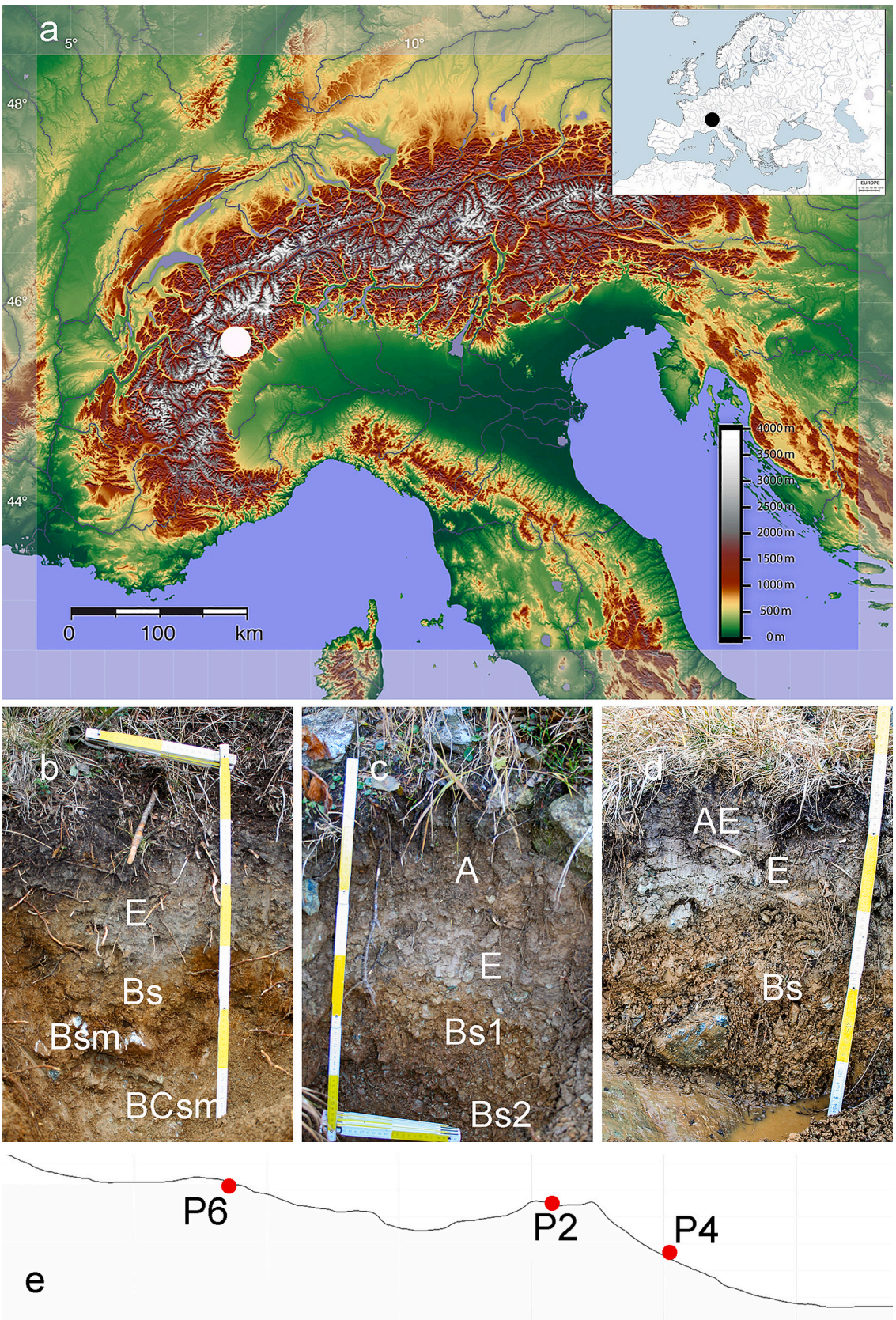

Fig. 1. Location of the studied soils in the NW Alps (a) and the three soil profiles (b-P2, c-P4 and d-P6); their location along the slope is shown in section e.

Table 1
Main topographic characteristics and lithological composition of the coarse fragments (%) in the deepest genetic horizon of each soil (> 5 mm).

Pedon	Slope %	Elevation m a.s.l.	Serpentinite	Metagabbro	Prasinite	Amphibolite	Chlorite schist
P2	25	1830	10	80	7	2	1
P4	20	1975	80	10	1	3	6
P6	18	2117	85	4	10	0	1

following the same procedure adopted for Mg-saturation, and X-rayed. After K saturation, vermiculites become visible (migration of part of the 1.4 nm peak to 1.0 nm). The K-saturated mounts were then heated: at 350°C, HI minerals (Hydroxy-Interlayered) appear (decrease of the 1.4 nm peak intensity and increase of the intensity of the 1.0 nm one). Whether HI-minerals were HIV (HI vermiculites) or HIS (HI Smectites) was ascertained by comparing the Mg-EG and K-heated samples. Further heating to 550°C allowed to assess the presence of kaolinite, which was detected due to the disappearance of the 0.712 nm peak upon heating. The serpentine minerals were recognized from the 0.72–0.73 nm peak. Peaks were identified with X'Pert Highscore software (2005). Digitized X-ray data were smoothed and corrected for Lorentz and polarization factors (Moore and Reynolds, 1997). The area underlined by the peak line was used for the semi-quantitative clay analysis.

The sand fraction, obtained after wet sieving (> 0.1 mm), was analyzed using XRD as well, on powder samples, using the same instrument as previously described, but scanning the randomly oriented samples from 2 to 60°2θ (steps of 0.02°2θ, 1 s/step).

Because of the potential presence of Fe-rich chlorite (odd-order peaks with decreased intensity upon heating, Wilson, 1987) the presence of kaolinite was also assessed by infrared spectroscopy. The clay samples for FT-IR (Fourier Transform Infrared Spectroscopy) were prepared as pellets using 1 mg of sample and 150 of KBr heated at 150°C, and spectra were recorded from 4000 to 250 cm^{-1}. In particular, the presence of kaolinite, tri- or di-octahedral occupancies and metal-hydroxylic groups were checked on FT-IR spectra of soil clays in the OH-stretching region (4000–3200 cm^{-1}) and in the M−O region (900–400 cm^{-1}), which were normalized using the minimum–maximum method and then compared to each other. The evaluation of the FT-IR spectra was performed using OPUS 6 software.

Imogolite-type materials (ITM, consisting of imogolite and proto-imogolite allophane) were estimated if the Al_{ox}-Al_p/Si_{ox} molar ratio was close to 2 (Al_{ox} and Si_{ox} are oxalate-extractable Al and Si, and Al_p is pyrophosphate-extractable Al, D'Amico et al., 2008), according to Parfitt and Henmi (1982):

$$ITM=(5 + 2.1*(Al_{ox}-Al_p)/Si_{ox}-1)*Si_{ox} \quad (1)$$

If the ratio is out of the 0.75–2.4 interval, the probability of existence of allophanic materials is extremely low (Egli et al., 2006).

Another method used for the assessment of active amorphous materials was the measurement of pH in a 1 N NaF solution, commonly used for the analysis of soils having andic properties: if the value is above 9.5, the presence of short range ordered materials is confirmed (Burt, 2004).

Magnetite was approximately quantified in the different horizons: 8–10 g of dry soil were crushed to a particle size smaller than fine sand and put on large glass plates where magnetite was removed with a hand magnet, cleaned and weighted. The process was replicated at least 5 times on each sample.

The elemental composition of some rock samples and of all genetic horizons was determined with XRF on pulverized samples (Spectro X-lab 2000).

2.3. Weathering and mass balance calculations

Mass transport calculations were performed according to the equations proposed by Egli and Fitze (2000):

$$\tau_{j,w}=(C_{j,w}C_{i,p}/C_{j,p}C_{i,w})-1 \quad (2)$$

where:

$\tau_{j,w}$: function of mass transport in the open system of *j* element, in the weathered material *w*;

$C_{j,w}$: concentration of the *j* element in the weathered material *w*;

$C_{i,p}$: concentration of the stable element *i* in the parent material *p*;

$C_{j,p}$: concentration of the *j* element in the parent material;

$C_{i,w}$: concentration of the stable *i* element in the weathered materials.

The strain (volume change in going from the morainic parent material to pedogenic horizons) was also calculated, hypothesizing a BD for the parent till equal to 1.80 g cm^{-3} (Musso et al., 2019), using the equation proposed by Chadwick et al. (1990):

$$\varepsilon_{i,w}=(\rho_p C_{i,p}/\rho_w C_{i,w})-1 \quad (3)$$

where:

$\varepsilon_{i,w}$: strain (volumetric change);

ρ_p: bulk density of the parent material;

ρ_w: bulk density of the soil horizons;

$C_{i,p}$: concentration of the stable element *i* in the parent material *p*;

$C_{i,w}$: concentration of the stable element *i* in the soil horizon;

Zr was taken as the stable element in the calculations, as Ti, although present in higher concentrations, is weakly mobile in acidic soils and in presence of chelating agents (Aide and Smith-Aide 2003). The C horizon is usually considered the parent material (Egli et al. 2006), but in this case a true C horizon was not sampled, because of the presence of hard rock (P6, P4) or pedogenic cementation (P2). The lithology of stone fragments (> 5 mm) of the deepest horizons was thus used to obtain the lithological composition (and thus the geochemical composition) of the original parent material of each soil profile, as in D'Amico et al. (2008).

To check whether aeolian additions have played some role in the mineralogical composition of the soils, the mass transport evaluation was also performed by including a potential contribution of Saharan dust to the soil parent material. Saharan dust was likely the dominant aeolian input in Central Europe throughout the Holocene (Stuut et al., 2009). Other potential dust sources, such as Late-glacial Alpine loess (e.g. Gild et al., 2018; Serra et al., 2020), cannot be excluded but no well-preserved layers of such materials have been identified in the NW Italian Alps. Tephra can also be ruled out: although volcanic ash from the Laacher See eruption (~13 ka BP) has been detected in lake varvae in the Alpine range (Finsinger et al., 2011), its contribution is minimal and considered almost negligible in terms of total aeolian inputs to soils (Mileti et al., 2013). The Saharan dust composition was obtained by averaging values from multiple sources (Goudie and Midleton, 2001; Moreno et al., 2006; Di Mauro et al., 2019; Scheuvens et al., 2013). Its input to soils in the Italian Alps was estimated from D'Amico et al. (2023), who calculated 86–146 kg m^{-2} of dust deposited during the Holocene in Podzols developed on dolostone in the Lombard Prealps. Considering the drier conditions of the Aosta Valley, which limit wet deposition, a conservative input of 60 kg·m^{-2} was used. This amount agrees with Varga et al. (2016) who calculated Saharan dust inputs as ca. 4 g m^{-2} yr^{-1} in Hungary, equal to ca. 41 kg m^{-2} during the Holocene. A much higher value (160 kg m^{-2}) of Saharan dust can be calculated from the data shown by Styllas et al. (2023) in Greek mountains, located in a much more southerly location. An aeolian input of 60 kg m^{-2} corresponds to ca. 20% of the total fine earth material, with slight variations among the six profiles, when the total mass of the fine earth was calculated from bulk density, thickness and stoniness of the different

horizons. Element balance, considering both dust inputs and parent rock weathering, was therefore also computed using a mixed parent material comprising 80% mafic or ultramafic rocks and 20% Saharan dust. The composition of this mixed parent material was calculated following Lawrence et al. (2013):

$$C_{jm}=C_{jd}\, f_d + C_{jr}(1\text{-}f_d) \quad (4)$$

Where:
C_{jm} is the concentration of element j in the mixed parent material;
C_{jd} isn the concentration of element j in the dust;
f_d is the mass fraction of dust in the fine earth fraction;
C_{jr} is the concentration of element j in the parent rock.

3. Results

3.1. Parent material characterization

The diffraction patterns of unweathered serpentinite fragments showed that this rock was composed mostly of antigorite, with small quantities (up to 3–4%) of magnetite and chromite (small peak at 0.252 nm and quantified after extraction with a hand magnet from the pulverized samples) (Fig. S1a, in Suppl. Mat.). The chlorite peaks (Fig. S1b) showed similar intensities of the odd and even order peaks. Only a small reduction in intensity was visible after heating, suggesting a primary Mg-rich, Fe-poor chlorite. In this mineral, Fe is usually well inserted in the 2:1 octahedral sheet, while Mg is situated in a more labile hydroxylic layer (Herbillon and Makumbi, 1975). Al is typically in the stable layers.

According to the XRD analysis (Fig. S1c), metagabbros were mostly composed of amphiboles (actinolite, 0.88 nm, and glaucophane at 0.83 nm), plagioclase (0.32 nm), chlorites, with minor quartz. Chlorite was similar to the one in the chlorite-schists (clinochlore), and it was probably particularly rich in Cr (Table 2).

The sand fraction of the different soil horizons, representing more than 50% of the soil material in mafic P2 and much less in the serpentine soils P4 and P6, showed the presence of mafic and ultramafic minerals in different proportions; quartz was usually in higher concentrations in surface horizons, together with hydrobiotite, while serpentine tended to be more concentrated in the deepest ones (Table 2).

3.2. Mineralogy of fine earth materials

3.2.1. XRD analysis of the clay fraction

Profile P2 (Table 3) displayed the typical clay mineralogical composition of Podzols (e.g. Egli et al., 2008), with the addition of small quantities of serpentine. Every horizon was characterized by a distinct clay assemblage compared to the ones above and below. In the least weathered BCsm horizon (Fig. S2a) only primary minerals (Chlorite – 1.41 nm, amphiboles – 0.83 nm, serpentine – 0.73 nm, talc – 9.3 nm, and traces of micas – 9.9 nm) were present. Chlorite closely resembled the primary mineral, with a slight Fe enrichment indicated by a minor decrease in secondary peaks after heating. The overlying Bsm horizon (Fig. 2c) had a similar clay mineralogy, but chlorite was richer in Fe evidenced by the strong reduction of the secondary peaks in 550°C heated samples. In addition, HIV was detected by the appearance of a peak at 1.02 in samples heated at 550°C. In the Bs horizon (Fig. 2b), slightly weathered minerals dominated over their pedogenic products: Fe-chlorite was the most common, followed by HIV and vermiculite. Large quantities of plagioclases and amphiboles were detected as well. The E horizon had a very different mineralogical composition, containing large amounts of smectites, vermiculites, HIV and Fe-chlorite (Fig. 2a).

The serpentinitic soils P4 and P6 (Table 3) exhibited extensive clay mineral weathering and transformation even in deep horizons. In the P4-Bs2 (Fig. S2b) and P6-Bs (Fig. 2i) horizons, serpentine minerals co-occurred with abundant pedogenic minerals, including smectite-chlorite intergrades (peak at 1.55 nm in EG-saturated samples), vermiculite, and HIV. Thin reddish films on stone fragments (D'Amico et al., 2008) indicated Fe-oxyhydroxide and clay illuviation. P4-Bs1 (Fig. 2f) was more weathered, and smectites were found. A, AE and E horizons had smaller serpentine amounts and a higher smectite, vermiculite and HIV content compared to the deeper horizons.

Kaolinite was detected in all horizons, except P2-BCsm. As its 001 peak overlaps the 002 of chlorite, together with the very strong reduction in intensity of the former in heated samples, its quantification will be treated in the section 3.2.4. Illite/mica was not detected in the Bs horizon of P6 in the other samples, its peak shifted from ca. 1.0 nm in the Bs horizons to 1.04 nm in A or E horizons. Quartz occurred in small amounts in all horizons (not shown). Talc was widespread, often more concentrated in the most weathered A, AE, E, and top Bs horizons. Lepidocrocite was present in all horizons except E (not shown).

3.2.2. Magnetic minerals

The A and/or Bs horizons of soils developed from serpentinite had the highest contents of magnetic minerals, either magnetite, chromite and/or intermediate spinels (Table 3). A strong weathering of these resistant minerals was shown by the great decrease in abundance in E horizons. The trend was the same for primary minerals in the clay fraction.

3.2.3. Imogolite-type materials

ITM (imogolite-type materials, including allophane, imogolite and proto-imogolite) are often found in podzolic soils. In P4 and P6, the (Al_o-Al_p)/Si_o molar ratio (Parfitt and Hemni, 1982) was well below 2 (D'Amico et al., 2008), suggesting that these materials should not be present in a significant amount. In the Bsm and BCsm horizons of P2, the equation gave around 1.8 and 1.2% for ITM, suggesting the presence of ITM minerals. Moreover, in the same horizons, pH (NaF) was above 10.6, which clearly demonstrated the presence of short range, imogolite-type materials.

3.2.4. FTIR measurements on the clay fraction

In all profiles, kaolinite was identified by the strong reflectance peaks at 3695 cm^{-1} and 3620 cm^{-1}, with the highest contents in E horizons and much lower ones in Bs ones (Table 4). The Bsm horizon of P2 and Bs2 of P4 contained little kaolinite (Fig. 3a, c), but its presence was confirmed by the peak at 916 cm^{-1} (Egli et al., 2001a), consistently visible though less intense in the same horizons.

Antigorite (absorption peak at 3671 cm^{-1}, Post and Borer, 2000) was abundant in the Bs horizons of P4 and P6 but not detected in A and E horizons, and the diagnostic peak was very weak in the deeper horizons of P2.

The strong reflectance peaks at ca. 3450 and 3620 cm^{-1} may correspond to interlayered Al hydroxides, with 3620 cm^{-1} also

Table 2
Proportion of the sand fraction and its semiquantitative mineralogical composition, derived from XRD analysis of the crushed coarse sand fraction. S = serpentine (mainly antigorite), C = chlorite, A = amphiboles (tremolite, actinolite), Q = quartz, P = plagioclase (albite), T = talc, M = micas, IB = hydrobiotite, Px = pyroxenes. Trace minerals are shown in brackets.

Pedon	Horizon	Sand %	Minerals
P2	E	51.2	C > P > Q≫(IB = M = T=S))
	Bs	57.5	C≫>≫S > P = A>>(T = M)
	Bsm	68.2	P=C > S > A≫(T > M)
	BCsm	71.9	P=C > S > A≫(T > M)
P4	A	40.7	S≫Q > C>(M = T = A)
	E	25.2	S≫Q≫(C > M > A = IB > T)
	Bs1	40.9	S≫>≫(C = Q>>M = T = A)
	Bs2	58.2	S≫>≫>(C = Q > M = T = A)
P6	AE	43.8	S≫C = A > Q > P≫(T > M = IB=Px)
	E	24.9	S > C = A > Q > P≫(T > M = IB=Px)
	Bs	49.6	S≫C = A≫P≫(Q = M > Px)

Table 3
Semi-quantitative composition of the clay fraction of the studied soils (****>50%, ***25–50%, **12–25%, *5–12%, +++3–5%, ++1–3%, + <1%) and magnetic mineral content (%) in the studied soil horizons.

Pedon	Hor.	* Serp	Chl	Smect.	HIS	Verm.	HIV	Amph	Plg.	Mica/ illite	Kao.	Talc	Qtz	Lep.	Magnetic Minerals (%)
P2	E	+	*	**	n.d.	*	**	n.d.	n.d.	+	+++	+	+	n.d.	0.92
	Bs	+++	***	n.d.	n.d.	*	**	+	++	+	*	++	++	+	0.86
	Bsm	**	***	n.d.	n.d.	n.d.	*	++	++	+	***	+	++	+	0.80
	BCsm	**	****	n.d.	n.d.	n.d.	n.d.	*	*	+	n.d.	++	++	+	1.30
P4	A	**	*	**	n.d.	**	n.d.	n.d.	n.d.	++	**	*	*	++	4.20
	E	**	*	***	n.d.	+	**	n.d.	n.d.	+++	*	++	++	+	2.57
	Bs1	**	**	**	n.d.	**	**	n.d.	n.d.	+++	*	++	++	++	4.10
	Bs2	***	**	n.d.	**	*	++	n.d.	n.d.	++	**	+	++	+++	5,45
P6	AE	**	**	**	n.d.	***	++	n.d.	n.d.	+++	*	+++	++	+	1.42
	E	**	**	***	n.d.	+++	n.d.	n.d.	n.d.	++	**	+++	++	+	1.03
	Bs	***	***	n.d.	*	+++	*	+	n.d.	n.d.	++	++	+	*	4.09

*Serp: serpentinite; Chl: chlorite; Smect: swelling mineral after EG solvation; HIS: hydroxy-interlayered chlorite-smectite (swelling to less than 1.6 nm after EG solvation); Verm: vermiculite; HIV: hydroxy-interlayered vermiculite; Amph: amphiboles; Plg: plagioclase; Kao: kaolinite; Qtz: quartz; Lep: lepidocrocite.

attributable to kaolinite (Egli et al., 2006), while the 3390 and 3525 cm^{-1} peaks were not visible. These peaks were more pronounced in E than in A or Bs horizons in all profiles and were almost not detectable in deep P2Bsm (Table 4).

The band at 3680 cm^{-1} appeared only in deep Bs horizons on serpentinite (P4 Bs2 and P6 Bs), confirming the scarcity of Mg-trioctahedral occupancies in highly weathered horizons (νMg_3OH, Caillaud et al., 2004).

In P4 and P6, the difference in the OH bending region (650–950 cm^{-1}) indicated a differential mineral weathering between horizons, The band at 650 cm^{-1}, indicative of octahedral Fe and Mg substitutions in 2:1 phyllosilicates, was weakly detectable only in Bs horizon in P6. The absorption bands at 830 cm^{-1} (AlMgOH) and 786 cm^{-1} (MgFeOH) decreased from the most weathered (E) to the least weathered (Bs, A) horizons. Higher quantities of Si-Al-O groups and quartz (779, 799 cm^{-1}) were evident in E horizons compared to Bs.

3.3. Geochemistry and mass transport calculations

The elemental composition of the fine earth samples distinctly differed from the parent material in all pedons (Table 5). In particular, the Ti/Zr ratio, which can indicate discontinuities or allochthonous materials (Munroe et al., 2024), remained relatively constant across soils and horizons, but was an order of magnitude higher in the parent material than in soils, with the lowest values in the E horizons.

Compared to the whole fine earth, the clay fraction showed a lower concentration of Mg, particularly in the deepest horizons (Table 5). Si did not show significant differences, while Al had higher concentration in P4 and lower in the others. Fe had higher concentrations in clays, as well as K, Ti and Zr.

Calculating the open-system mass transfer function τ based on the parent material composition (Table 3) and on the immobile element Zr revealed clearer weathering trends (Table 6). Despite uncertainties in estimating the precise parent material composition from the coarse fraction of the least weathered horizons, τ was negative for most elements, with Mg and Si showing the lowest values, which means they underwent the largest leaching losses. Al, Fe and Ca in P6 had slightly less negative functions. Al was residually enriched relative to Si (less negative τ), in the most weathered horizons on serpentinite, but not on mafic rocks, while Fe, Cr and Ni were more strongly leached on serpentinite. The volumetric strain ε was strongly negative, evidencing collapse of the material during pedogenesis.

If the presence of allochthonous materials is considered, the mass balance calculations deeply changed. Considering the addition of 60 kg m^{-2} of Saharan dust, the modified $*\tau$ remained negative for most elements except in the deepest spodic horizons (Table 7). The $*\tau$-values for Al_2O_3 and Fe_2O_3 were often positive, though lower in the E horizons than in other layers. The values for Ti were near zero in P2 and P4, while they remained strongly negative in P6. The volumetric strain was positive in P2 and in some horizons in P4 (indicating expansion) but stayed negative in most horizons of P4 and P6, with minimum values in E horizons.

4. Discussion

4.1. Soil mineralogy and weathering trends

Mineralogical properties confirmed the aggressive pedo-environment associated with the peculiar podzolization on ultramafic materials (D'Amico et al., 2008). Podzolization is indeed linked to very low pH values, high exchangeable acidity, and intense water fluxes, as well as to a vegetation cover dominated by Ericaceae and conifers. This plant assemblage produces strongly acidifying litter and is typically associated with mycorrhizal, "rock-eating" fungi (Van Breemen et al., 2000). Dissolution is the dominant process affecting serpentine minerals (Dixon, 1989; Lee et al., 2003; Schreier et al., 1987), explaining the extreme Mg and Si losses and the marked reduction of serpentine in the clay fraction from the least to the most weathered soil horizons. FTIR and XRD analyses confirmed the near-complete serpentine disappearance from the clay fraction in the most weathered horizons, leaving residual chlorite or other Al-rich phyllosilicates. In temperate environments, ultramafic rocks usually weather to oxidic rather than clay silicate materials thanks to the predominant dissolution of serpentine minerals and the residual concentration of metal oxides (Buurman et al., 1988). In the studied subalpine soils, podzolization removed the oxides from near-surface horizons, enabling the formation of an E horizon. Consequently, most clays found in serpentine soils in subalpine habitats derive from the transformation of primary trioctahedral chlorites into dioctahedral smectite, vermiculite and hydroxy-interlayered minerals (Buurman et al., 1988), following the typical chlorite weathering pathway in Podzols (Carnicelli et al., 1997; Mirabella and Egli, 2003).

The first processes affecting primary Mg-rich trioctahedral chlorite (clinochlore) is Fe oxidation, which disrupts the mineral structure and causes the loss of the Mg-rich brucitic interlayer sheet. The free interlayer space becomes accessible to Al (and Fe, in Fe-rich soils) deposition. Mg may also be leached from the 2:1 octahedral sheet and replaced by Al (Carnicelli et al., 1997; Mirabella and Egli 2003). These transformations mark the onset of the trioctahedral-to-dioctahedral transition. XRD analyses confirmed the early transformation of primary Mg-rich chlorites into pedogenic Fe-rich chlorite in the studied mafic and ultramafic soils. In the deepest BCsm horizon of profile P2, chlorite showed a pattern similar to the primary, Mg-rich one (detected in both chlorite-schists and gabbro), while in the overlying Bsm and most Bs horizons, heating to 550°C caused secondary peaks to nearly disappear and increased the differentiation between 001, 003, 005 and 002, 004 peaks (Fig. 2, Fig. S1). This indicated Fe enrichment in weathered, or pedogenic,

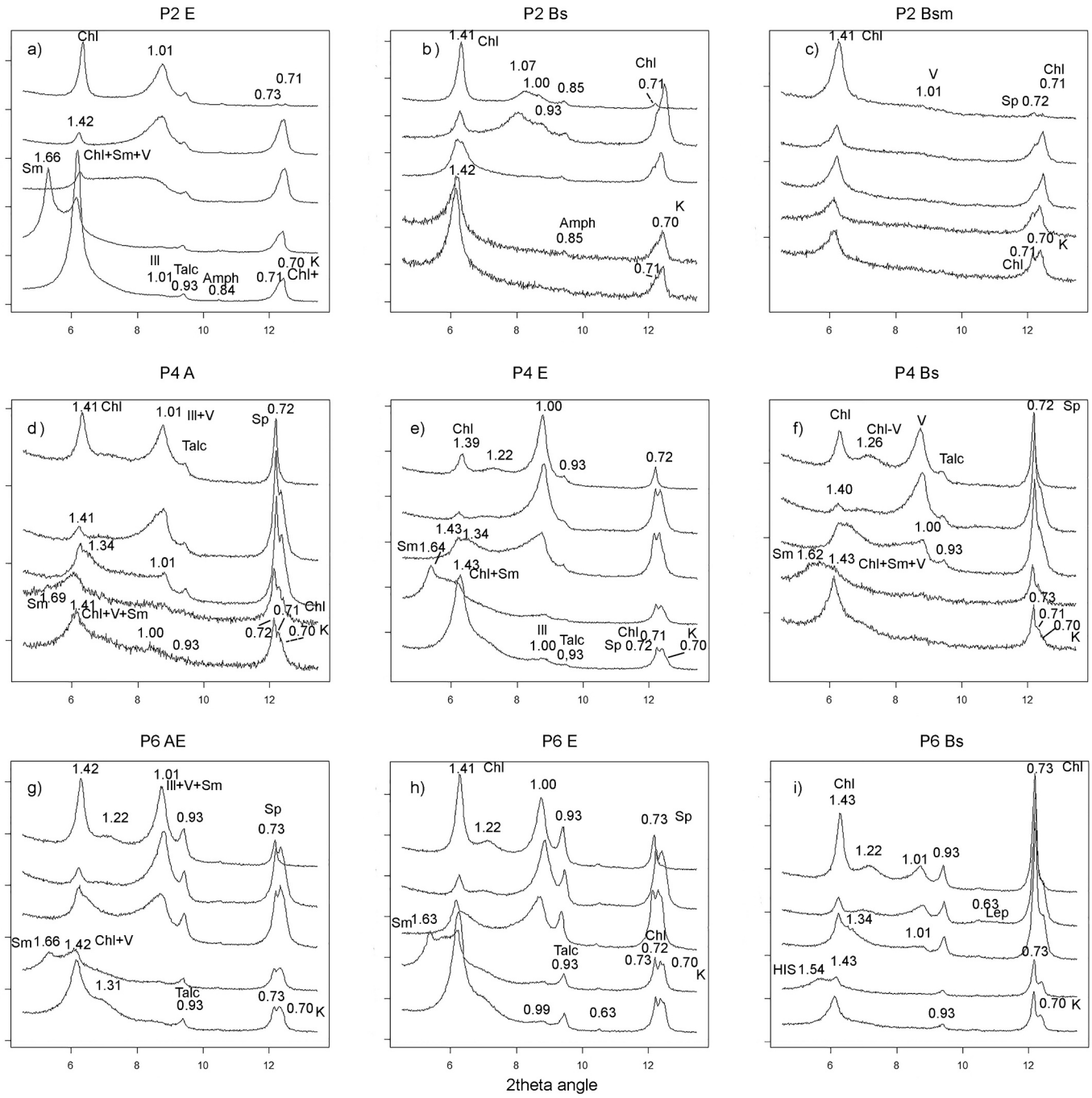

Fig. 2. XRD diffraction patterns of the clay fraction of selected horizons. In each graph, from the bottom line to the top one, are shown: Mg-saturated clay, clay samples after ethylene glycol solvation, K-saturated clays, and clays after heating to 335° and 550°C. Only the section between 3 and 13.5 ° 2ϑ is shown, where the 001 and 002 peaks of most clay minerals are observed

chlorites (Wilson, 1987). Iron and/or Al occupying vacant positions likely originated from weathering driven by complexing organic acids produced by subalpine vegetation.

In the Bs horizons, hydroxy-interlayered minerals and vermiculite appeared, which represent the second step in chlorite weathering (Fig. 2). Trioctahedral occupancies were still common, according to the IR spectra (Fig. 3). On serpentinite, smectites (P4Bs1) and chlorite-smectite interlayered minerals (P4Bs2 and P6Bs) indicated intense leaching, typical for E horizons (Egli et al., 2001a).

In the most weathered E horizons, significant Mg depletion from the clay mineral structure led to the abundance of dioctahedral vermiculites and smectites. The presence of Al- and Fe-rich smectites (beidellites and montmorillonites) is likely, based on mass balance calculations and on clay fraction composition (Table 5). As Mg and Si are usually strongly leached, Al tends to accumulate residually in the < 2 mm fraction in highly weathered horizons on ultramafic materials (Bonifacio et al., 1997; Bulmer, 1992; Kierczak et al., 2007; Lee et al., 2003; Noack and Colin 1986; Rabenhorst et al., 1982). This accumulation reflects the greater stability of Al-bearing minerals such as chlorite (and its weathering derivatives) and amphiboles compared to serpentine. The relatively constant Al content with depth is explained by its incorporation in primary Mg-chlorites and their weathering products, including Fe-chlorites, hydroxy-interlayered minerals (HIS, HIV), smectites, and vermiculites (Caillaud et al., 2006).

Table 4
Main ftir bands observed in the analyzed soil samples and reference (+++ strong absorption peak, ++ moderate peak, + small peak,− trace).

Band cm^{-1}	Mineral/group	Reference	P2 E	P2 Bs	P2 Bsm	P4 A	P4 E	P4 Bs2	P6 E	P6 Bs
3695	Kaolinite	Egli et al., 2001a	+++	+++	+	+++	+++	++	+++	++
3680	Mg-trioctahedral occupancy	Caillaud et al., 2004	n.d.	n.d.	n.d.	−	n.d.	+++	n.d.	+++
3671	Antigorite	Post and Borer, 2000	n.d.	−	+	n.d.	n.d.	++	n.d.	++
3620	Kaolinite	Egli et al., 2001a	+++	+++	+++	+++	+++	++	+++	+++
3620	Interlayer Al-hydroxides	Egli et al., 2006	+++	+++	+++	+++	+++	++	+++	+++
3525	Interlayer Al-hydroxides	Egli et al., 2006	n.d.	n.d.	n.d	n.d.	n.d.	n.d	n.d.	n.d
3450	Interlayer Al-hydroxides	Egli et al., 2006	+++	+++	n.d.	++	++	++	+++	++
3390	Interlayer Al-hydroxides	Egli et al., 2006	n.d.	n.d.	n.d.	n.d.	n.d.	n.d.	n.d.	n.d.
916	Kaolinite	Egli et al, 2001a	+++	+++	++	++	++	n.d.	++	+
830	δ_{AlMgOH}	Egli et al, 2001a	−	−	−	−	−	−	−	−
786	δ_{FeMgOH}	Egli et al, 2007	n.d.	n.d.	n.d.	n.d.	n.d.	n.d.	n.d.	n.d.
799	Si-Al-O and quartz	Egli et al., 2007	+++	+++	+++	++	++	+	+++	++
779	Si-Al-O and quartz	Egli et al., 2007	++	++	++	++	++	+	++	+
650	Fe/Mg octahedral substitution	Egli et al., 2006	n.d.	n.d.	n.d.	n.d.	n.d.	n.d.	n.d.	−

The weathering end-product of chlorite is probably kaolinite, which was detected by both XRD and IR spectra, particularly in E and AE horizons. Smectite (particularly beidellite) transformation into kaolinite in acidic soils was demonstrated by Karathanasis and Hajek (1983) and supported by Spinola et al. (2022), while others (e.g. Mirabella and Egli, 2003) stated that the rare occurrence of kaolinite in podzolic E horizons is owing to the young age of Alpine soils and not primarily due to thermodynamic limitations. In the mafic profile P2, the appreciable concentrations of kaolinite also in deeper horizons could be due to plagioclase weathering (Egli et al., 2001a).

Serpentine soils are often characterized by the presence of Mg-smectites, particularly in concave topographic positions, formed by neogenesis from the ions derived from mineral dissolution upstream (Bonifacio et al., 1997; Bani et al., 2014). In the studied soils, because of the ongoing podzolization, Mg and Si are easily leached out of the profiles (as demonstrated by mass transfer functions), while some Al is deposited in deeper illuvial Bs horizons. Thus, the presence of smectite can only be related to the weathering processes of Al-bearing minerals (as normally happens during podzolization).

Talc and spinels are other common rock-forming minerals in serpentinites worldwide. Talc had the highest concentration in the most weathered horizons. This might be caused by the lower octahedral to tetrahedral ratio slowing down its dissolution in acidic environments (Ducloux et al., 1976; Lin and Clemency, 1981; Bales and Morgan, 1985; Freyssinet and Farah, 2000) and, thus, increasing its residual concentration in the most weathered layers. Resistant magnetite and chromite (and possible intermediate forms) had an opposite trend, with the lowest contents in the most weathered horizons. Their dissolution has been demonstrated in hydromorphic soils (Fisher et al., 2008), but there is no evidence in literature of their weathering in extremely acidic podzolic soils because of low pH values and / or chelating organic acids.

The cementing agent of the deep Bsm and BCsm horizons in the mafic profile P2 was probably composed of ITMs (Pilar et al., 2024), produced by the dissolution of easily weatherable mafic and ultramafic primary minerals and the consequent Si release in solution. Mass balance calculations also showed that Si was accumulated in these cemented horizons (Table 6).

Thus, clay mineralogy is well in agreement with the podzolic weathering and leaching trends in these ophiolitic soils.

However, the abundance of quartz and mica/illite might indicate the presence of allochthonous materials, as mafic and ultramafic rocks host only trace amounts of such minerals. Although the strong weathering environment does not allow the persistence of typical clay minerals deriving from Saharan dust, such as palygorskite and calcite (Guerzoni et al., 1997, Rodriguez-Navarro et al., 2018), some of the detected kaolinite might have an aeolian origin as well.

4.2. Aeolian inputs and weathering trends

As shown in the previous sections, mass balance calculations reveal extreme leaching of most elements, with Mg and Si losses reaching 67–99% (Table 6). Even Al, despite its higher concentration in the soil than in the parent material, showed substantial depletion when compared to Zr (Table 6). Such element losses would have given rise to a significant topographic lowering (up to 8 m) since the end of the Pleistocene glaciation; these values would be comparable to the ones measured in Podzols on dolostone (D'Amico et al., 2023). However, it seems highly unlikely that a surface lowering of 8 m has taken place since the surface became ice-free (about 15–18 ka). By contrast, podzolic soils on sialic materials typically show much lower element losses (40–60% for Mg, Egli et al., 2006). Very high losses of dissolved materials (up to 64%) have been observed also by other authors in less extreme edaphic conditions, such as the serpentinitic outcrops in Maryland (Cleaves et al., 1974), or even close to 100% in 1 Ma old soils on basalt in Hawaiian topsoils (Porder et al., 2007). High dissolved Si in leachates below podzolic E horizons has been measured by Ugolini et al. (1977), implying large Si losses. The extreme values in our soils are consistent with their high Zr content, which is 3 orders of magnitude higher than in the parent material. Without considering external inputs, it is hard to believe in such values. In fact, stable element ratios (Table 6) suggest substantial dust input. In particular, the Ti/Zr ratio in the soils was an order of magnitude lower than in the parent rock but closely matched reported the values for dust (Goudie and Midleton, 2001; Moreno et al., 2006; Di Mauro et al., 2019; Scheuvens et al., 2013). In the clay fraction, the Ti/Zr ratio was nearly identical to that of Saharan dust.

In fact, Saharan dust deposition has occurred for thousands of years, at least since the desertification of the Sahara Desert around 5000–4200 BP (Kröpelin et al., 2008; Boxleitner et al., 2017). Saharan dust contains on average 324 mg kg^{-1} Zr (Moreno et al., 2006), two to three orders of magnitude higher than the parent material of the studied soils. Zr losses in the soil profiles can be excluded, as all other elements were less enriched, and even the slightly more mobile Ti showed an order of magnitude lower enrichment than Zr.

Assuming 60 kg m^{-2} of Saharan dust inputs over 5–8 ka, equal to ca. 20% of the soil mass, mass transfer functions became less negative, or even positive for some elements in specific horizons. The obtained τ values agree with the intense podzolization processes, marked by maximum mass losses in E horizons and some accumulations in Bs ones, particularly Al in P2, Fe in P2 and P4, and almost no net Si loss from cemented P2 Bsm, in agreement with the presence of illuvial amorphous silica or ITMs as cementing agent (Alexander et al., 1994). Estimated fine earth losses amount to 39 kg m^{-2} in mafic P2 and 175–170 kg m^{-2} in ultramafic P4 and P6, corresponding to ~ 13% and 70–73% of fine earth removal since postglacial soil formation. These amounts agree

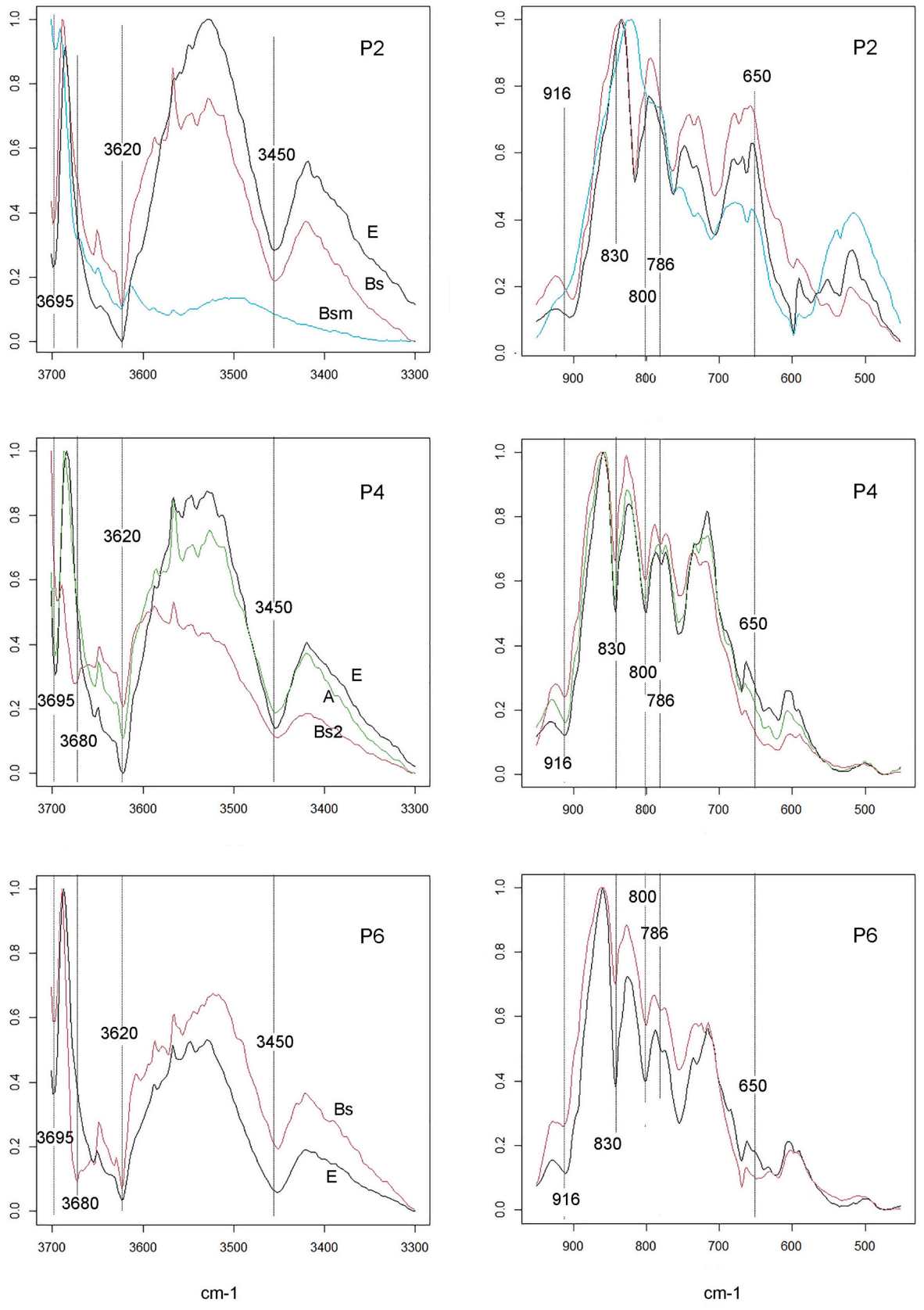

Fig. 3. OH stretching and bending region of the different horizons in the different soil profiles, min-max-normalized. Some reflectance bands, characteristic for clay minerals, are shown. On the left, the OH-bending region, on the right the OH-stretching region.

Table 5
Elemental composition of the parent material as calculated from the coarse fraction composition (D'Amico et al., 2008) in the least weathered horizon, ratio between element concentration in the horizon and in the parent material (expressed as %), ratio between immobile Ti and Zr. *: Saharan dust composition is averaged from several works (Goudie and Middleton, 2001; Moreno et al., 2006; Di Mauro et al., 2019; Scheuvens et al., 2013).

	MgO	Al_2O_3	SiO_2	K_2O	CaO	MnO	Fe_2O_3	P	Ni	Cr	Ti	Zr	Ti/Zr
	%	%	%	%	%	%	%	mg kg^{-1}	mg kg^{-1}	mg kg^{-1}	mg kg^{-1}	mg kg^{-1}	
Rock samples													
Serpentinite	41.89	0.64	42.44	0.00	0.05	0.11	11.90	4.2	1325	4532	11.7	0.09	130.2
Chloriteschist	32.05	27.93	31.48	0.01	2.13	0.11	12.98	55.3	1274	2383	154.4	1.75	88.2
Metagabbro	15.60	15.7	46.10	0.03	10.50	0.06	4.30	106.6	310	2654	1299.6	7.15	181.8
Metabasalt	18.20	10.6	42.40	0.02	7.60	0.21	10.6	238.5	284	506	17696.2	71.55	247.3
Amphibolite	31.00	11.8	36.20	0.01	7.80	0.17	7.80	86.0	1389	860	275.0	1.75	157.1
Parent material													
P2	36.32	5.86	46.78	0.03	3.62	0.10	6.16	0.02	895.6	2375.9	873.9	4.55	191.9
P4	41.65	3.43	46.03	0.03	1.58	0.11	6.47	0.01	1076.4	2525.4	473.4	2.69	176.2
P6	42.00	2.29	46.46	0.03	1.37	0.13	6.94	0.02	1046.9	1485.7	2082.9	9.13	228.2
Saharan Dust													
	3.21	14.49	61.89	2.74	8.96	0.07	6.64	0.11	36.5	128.2	6641.5	270.9	24.5
Element concentration in soil horizons													
P2E	15.74	16.19	54.61	0.60	6.85	0.07	4.80	0.01	375.9	974.5	2768.6	87.7	31.6
P2Bs	18.04	17.47	48.48	0.59	5.75	0.08	8.92	0.03	474.8	1200.5	3025.2	78.8	38.4
P2Bsm	20.50	19.09	45.66	0.68	4.88	0.08	8.58	0.03	726.2	1302.3	2383.1	71.9	33.2
P2BCsm	21.90	17.26	46.31	0.28	7.03	0.07	6.36	0.02	672.6	1126.4	1470.0	31.3	46.9
P4A	30.15	7.62	47.79	0.80	0.92	0.22	11.66	0.05	1268.9	3317.4	2603.0	73.8	35.3
P4E	26.74	8.83	52.62	1.03	1.17	0.11	8.73	0.03	684.5	2794.4	3261.2	133.9	24.4
P4Bs	30.70	6.88	48.62	0.81	1.16	0.13	10.97	0.02	925.2	2980.9	2491.8	93.8	26.6
P4CBs	32.63	6.32	47.47	0.68	1.25	0.15	10.79	0.03	962.9	3065.8	2296.1	73.6	31.2
P6AE	20.50	11.26	55.71	1.00	3.76	0.11	6.88	0.03	394.3	1614.2	4731.8	176.2	26.9
P6E	20.68	10.54	56.31	0.90	4.50	0.10	6.25	0.02	375.5	1527.3	4418.3	185.1	23.9
P6Bs	27.25	8.58	48.90	0.34	4.76	0.12	9.38	0.02	644.2	2049.0	3248.1	95.9	34.2
Element concentration in the clay fraction													
P2E	7.26	12.89	54.51	1.37	2.62	0.13	9.72	–	–	–	5420	244	22.2
P2Bs	6.37	13.73	57.90	1.52	2.50	0.10	8.74	–	–	–	5720	259	22.1
P2Bsm	7.69	13.74	54.28	1.32	2.16	0.13	11.66	–	–	–	5870	370	15.9
P2BCsm	6.29	15.87	51.67	1.83	1.90	0.21	12.05	–	–	–	6340	267	23.8
P4A	7.37	15.11	51.04	1.67	2.21	0.22	12.57	–	–	–	5910	200	29.5
P4E	9.31	13.94	48.53	1.43	2.63	0.27	13.64	–	–	–	5430	163	33.4
P4Bs	11.42	12.45	44.27	1.19	2.91	0.30	16.92	–	–	–	4970	163	30.5
P4CBs	25.41	4.58	40.99	0.13	2.46	0.21	12.39	–	–	–	1580	145	10.9
P6AE	25.53	3.97	42.47	0.09	1.89	0.22	13.30	–	–	–	1290	143	9.0
P6E	11.67	11.78	45.17	0.84	2.49	0.27	16.31	–	–	–	4270	155	27.5
P6Bs	21.23	7.75	40.24	0.34	1.86	0.27	15.63	–	–	–	2580	147	17.6

Table 6
open system mass transport functions (τ_{Zr}) and volumetric strain ε_{Zr} of the main elements in the three studied soils, based on immobile Zr. BD: Bulk density, g cm^{-3}.

τ_{Zr}	MgO	Al_2O_3	SiO_2	CaO	Fe_2O_3	P_2O_5	Ni	Cr	BD	ε_{Zr}
P2E	−0.98	−0.86	−0.94	−0.90	−0.96	−0.95	−0.98	−0.98	0.96	−0.91
P2Bs	−0.97	−0.83	−0.94	−0.91	−0.92	−0.89	−0.97	−0.97	1.21	−0.92
P2 Bsm	−0.96	−0.79	−0.94	−0.91	−0.91	−0.88	−0.95	−0.97	1.25	−0.92
P2 BCsm	−0.95	−0.75	−0.92	−0.62	−0.92	−0.90	−0.95	−0.96	1.31	−0.89
P4AE	−0.97	−0.92	−0.96	−0.98	−0.93	−0.86	−0.96	−0.95	0.88	−0.93
P4E	−0.99	−0.95	−0.98	−0.99	−0.97	−0.95	−0.99	−0.98	0.77	−0.96
P4Bs1	−0.98	−0.94	−0.97	−0.98	−0.95	−0.95	−0.98	−0.97	1.22	−0.96
P4Bs2	−0.97	−0.93	−0.96	−0.97	−0.94	−0.93	−0.97	−0.96	1.42	−0.96
P6AE	−0.97	−0.75	−0.94	−0.86	−0.95	−0.90	−0.98	−0.97	0.68	−0.87
P6E	−0.98	−0.77	−0.94	−0.84	−0.96	−0.94	−0.98	−0.97	0.98	−0.92
P6Bs	−0.94	−0.64	−0.90	−0.67	−0.87	−0.91	−0.94	−0.92	1.12	−0.86

Table 7
Mass transfer function *τ, considering the addition of 60 kg m^{-2} of Saharan dust, corresponding to ca. 20% of the fine earth mass in each profile.

$*\tau_{Zr}$	NaO_2	MgO	Al_2O_3	SiO_2	K_2O	CaO	MnO	Fe_2O_3	P_2O_5	Ni	Cr	Ti	$*\varepsilon_{Zr}$
P2E	−0.40	−0.65	0.41	−0.28	−0.31	−0.04	−0.56	−0.49	−0.72	−0.66	−0.67	−0.10	0.10
P2Bs	−0.83	−0.55	0.69	−0.29	−0.25	−0.10	−0.43	0.05	−0.37	−0.52	−0.54	0.10	−0.03
P2Bsm	−0.94	−0.44	1.02	−0.26	−0.05	−0.16	−0.33	0.10	−0.26	−0.19	−0.46	−0.05	0.03
P2BCsm	−0.40	−0.32	1.59	−0.02	−0.12	2.02	−0.28	0.01	−0.30	−0.28	−0.49	0.05	0.14
P4A	−0.91	−0.32	0.03	−0.26	0.07	−0.77	0.64	0.37	0.25	0.12	0.24	0.16	0.39
P4E	−0.96	−0.67	−0.34	−0.55	−0.24	−0.84	−0.55	−0.44	−0.57	−0.67	−0.43	−0.20	−0.13
P4Bs	−0.94	−0.46	−0.27	−0.41	−0.15	−0.77	−0.23	0.01	−0.55	−0.36	−0.13	−0.12	−0.21
P4CBs	−0.92	−0.26	−0.14	−0.26	−0.09	−0.69	0.10	0.27	−0.41	−0.15	0.15	0.03	−0.14
P6AE	−0.95	−0.79	−0.17	−0.61	−0.39	−0.55	−0.66	−0.65	−0.67	−0.84	−0.72	−0.45	−0.18
P6E	−0.96	−0.80	−0.26	−0.62	−0.48	−0.48	−0.70	−0.70	−0.81	−0.85	−0.75	−0.51	−0.46
P6Bs	−0.91	−0.48	0.18	−0.36	−0.61	0.07	−0.35	−0.12	−0.71	−0.51	−0.34	−0.30	−0.07

with the high solubility of serpentine minerals in acidic soil environment and the more resistant mafic parent material in P2. They also agree with the much higher sand content in profile P2 than in P4 and P6, evidencing much lower dissolution rates in mafic materials (Brimhall and Dietrich, 1987).

Volumetric strain provides additional insights into the weathering pathways in the studied soils. When aeolian inputs are not considered, volumetric strain (ε_{Zr}) is strongly negative, as shown in Table 6, indicating substantial collapse during pedogenesis, locally exceeding 90% relative to the parent till. These values are obtained despite the relatively low bulk density of the soils (<1.4 g cm^{-3} in most horizons and $<$ 1 g cm^{-3} in the A and E horizons), as well as the significant input of organic matter, roots, and biological activity, increasing porosity, observed in the field. Such factors are generally associated with volumetric dilation rather than collapse (e.g. Jersak et al., 1995; Egli et al., 2001b). Strong elemental depletion is typically linked to negative volumetric strain in old soils, whereas Holocene soils are generally characterized by dilation, with the exception of a few strongly leached E horizons (Brimhall et al., 1992; Eger et al., 2011). Incorporating aeolian inputs into the mass-balance calculations yields results that are more consistent with values reported in the literature (Table 7).

Other potential dust sources cannot be excluded, such as late-glacial local dust, which has been documented in Alpine soils (Küfmann, 2003; Gild et al., 2018; Serra et al., 2021). This material, however, is better preserved as distinct soil layers on limestones (Küfmann, 2003; Gild et al., 2018). On different substrates, their geochemical composition does not allow for a clear differentiation from Saharan dust (D'Amico et al., 2023).

Studying weathering and geochemical mass balance in soils on Al-poor substrates thus allowed us to conclude that Saharan dust inputs are able to modify soil geochemistry and thus enhance some pedogenic trends (i.e. podzolization) on Holocene scale, even though dust inputs in the Alps have often been considered not detectable in soils (e.g. Egli et al., 2008; D'Amico et al., 2016). Similarly, Al and silica contents detected in mid-latitude soils developed on ultramafic rocks might have aeolian origin as well (e.g. Sasaki et al., 1968; Gasser et al., 1994).

4.3. Nutrients and trace elements mass transfer function vs the "serpentine factor"

Despite what normally happens in serpentine soils in temperate climates (e.g., Alexander, 1988; Bonifacio et al., 2013; D'Amico et al., 2014; D'Amico et al., 2020), no significant biocycling of P, Ca and K occurred in surface horizons, as shown by mass balance calculations. Typically, P and Ca bioaccumulation, coupled with Mg loss, mitigates the "serpentine factor" over time (Alexander, 1988; D'Amico et al., 2020), but the extreme leaching in these podzolic soils prevented Ca accumulation.

Ni was strongly leached from surface horizons: this metal is mostly included in easily weatherable serpentine minerals (Kierczak et al., 2021), and a certain extent of leaching is expected since the first stages of soil formation even in drier alpine environments (Bonifacio et al., 2013). Cr, however, also experienced unusually strong leaching, which is rare even in subalpine or boreal soils (Bulmer, 1992). Fe was mobilized as well. The mobility of Cr and Fe, normally retained in surface horizons of serpentine soils, likely results from extreme acidification driven by vegetation, the subalpine wet and cold climate, and complexing agents associated with podzolization. The role of organic acids in removing heavy metals (including Fe and Cr) has been demonstrated by Schreier et al (1987). In addition, Fe loss was particularly strong in P6, where seasonal waterlogging frequently occurred due to shallow rocky substrates.

Kierczak et al. (2007) showed how climate affects Ni and Cr mobility in temperate soils: humidity enhances Mg and Ni leaching, by decreasing the pH, while at the driest sites Ni was more stable and only Mg was diminished in the soil horizons. In the strong weathering environment found in subalpine forests, with precipitation values around 1000 mm, a deep and long-lasting snow cover and frequent summer rainfalls, associated with mean yearly temperature between 0° and 3°C, also the least mobile elements were mobilized (i.e. Cr).

Ni and Cr losses align with mineral weathering patterns. In fact, Ni and Cr (Manceau et al., 1985, de Caritat et al. 1993) are often located in the octahedral sheet of chlorite, substituting for Mg or Fe^{2+}. The octahedral layer in trioctahedral chlorite is the most susceptible to weathering, as demonstrated by the early transformation from Mg to Fe-rich mineral. An early release of heavy metals derived from chlorite weathering is highly probable. It is however possible that Ni and Cr are conserved in the octahedral sheet during Fe substitution for Mg and are later released by subsequent pedogenic processes. The conservation of heavy metals through the weathering stages of serpentine is demonstrated by Caillaud et al. (2009), but in that case the soil and environmental characteristics were different from the ones observed in subalpine forests (pH values around 7, low metal mobility and leaching). However, the extreme acidity of the subalpine pedo-environment accelerates serpentine dissolution, releasing Ni^{2+}, which substitutes Mg^{2+} due to similar ionic size and charge.

Negative mass transfer function values for Ni and Cr indicate that large quantities of these potentially toxic elements are released from these soils to surface and ground waters. This agrees with the high Ni and Cr contents measured in a nearby ombrotrophic peat bog surrounded by the same subalpine forest not far from P4, likely derived from stream and spring waters (Pavan et al., 2016).

5. Conclusions

All our working hypotheses have been verified. In fact, the results of this study suggest that podzolization creates a highly aggressive pedoenvironment capable of substantially modifying soils developed on serpentinite. This environment appears to promote extensive dissolution of serpentine minerals and the progressive transformation of chlorite and other mafic minerals into pedogenic clay phases, following the typical podzolization weathering pathways even on ultramafic substrates (Hypothesis a). The observed mineralogical transformations and mass balance calculations imply significant element mobilization during soil development. Trace-element fluxes show that up to 85% of Ni and up to 75% of Cr were mobilized and leached, thanks to the podzolization process (Hypothesis b). Mass-balance calculations further indicate that weathering of the parent material alone is insufficient to account for the present geochemical composition of the soils. This discrepancy points to the contribution of externally derived material, most plausibly aeolian inputs, with Saharan dust representing a likely dominant source and potential additional contributions from late-glacial local loess. While the exact magnitude of these inputs remains uncertain, and processes such as erosion were not explicitly addressed, the results suggest that aeolian deposition has played an important role in influencing the geochemical evolution of podzolic soils developed on atypical parent materials (Hypothesis c). This result explicates the observed Al and Si enrichment in many soils developed from ultramafic materials worldwide.

CRediT authorship contribution statement

Michele E. D'Amico: . **E. Bonifacio:** Writing – review & editing, Validation, Formal analysis, Data curation, Conceptualization. **A. Cavallo:** Writing – review & editing, Formal analysis. **M. Egli:** Writing – review & editing, Validation, Formal analysis, Data curation. **F. Previtali:** Writing – review & editing, Supervision, Project administration.

Funding

This research did not receive any specific grant from funding agencies in the public, commercial, or not-for-profit sectors.

Declaration of competing interest

The authors declare that they have no known competing financial interests or personal relationships that could have appeared to influence the work reported in this paper.

Acknowledgements

We thank Fabio Moia and Davide Cantelli for many of the lab analysis, and the former Director of Mont Avic Natural Park, Massimo Bocca, for the economic support of this project.

Appendix A. Supplementary data

Supplementary data to this article can be found online at https://doi.org/10.1016/j.geoderma.2026.117772.

Data availability

No data was used for the research described in the article.

References

Aide, M., Smith-Aide, C., 2003. Assessing soil genesis by rare elemental analysis. Soil Sci. Soc. Am. J. 67, 1470–1476. https://doi.org/10.2136/sssaj2003.1470.

Alexander, E.B., 1988. Morphology, fertility and classification of productive soils on serpentinized peridotites in California (U.S.A.). Geoderma 41, 337–351. https://doi.org/10.1016/0016-7061(88)90069-9.

Alexander, E.B., Graham, R.C., Ping, C.L., 1994. Cemented ultramafic till beneath a podzol in southeast Alaska. Soil Sci. 157, 53–58.

Arobba, D., Brugiapaglia, E., Gianotti, F., Siniscalco, C., Caramiello, R., Mercalli, L., Cat Berro, D., 2016. Cambiamenti climatici e della vegetazione sulla base di analisi litoe biostratigrafiche della Torbiera di Pian Pessey (Parco Naturale del Mont Avic, Valle d'Aosta). Nimbus 75, 8–28.

Bales, R.C., Morgan, J.J., 1985. Dissolution kinetics of chrysotile at pH 7 to 10. Geochim. Cosmochim. Acta 49, 2281–2288. https://doi.org/10.1016/0016-7037(85)90228-5.

Bani, A., Echevarria, G., Montargès-Pelletier, E., Gjoka, F., Sulçe, S., Morel, J.L., 2014. Pedogenesis and nickel biogeochemistry in a typical Albanian ultramafic toposequence. Environ. Monit. Assess. 186, 4431–4442. https://doi.org/10.1007/s10661-014-3709-6.

Bonifacio, E., Zanini, E., Boero, W., Franchini-Angela, M., 1997. Pedogenesis in a soil catena on serpentinite in north-western Italy. Geoderma 75, 33–51. https://doi.org/10.1016/S0016-7061(96)00076-6.

Bonifacio, E., Falsone, G., Catoni, M., 2013. Influence of serpentine abundance on the vertical distribution of available elements in soils. Plant and Soil 368, 493–506. https://doi.org/10.1007/s11104-012-1530-y.

Boxleitner, M., Musso, A., Waroszewski, J., Makiewicz, M., Maisch, M., Dahms, D., Brandová, D., Christl, M., de Castro Portes, R., Egli, M., 2017. Late Pleistocene – Holocene surface processes and landscape evolution in the central Swiss Alps. Geomorphol 295, 306–322. https://doi.org/10.1016/j.geomorph.2017.07.006.

Brimhall, G.H., Dietrich, W.E., 1987. Constitutive mass balance relations between chemical composition, volume, density, porosity, and strain in metasomatic hydrochemical systems: results on weathering and pedogenesis. Geochim. Cosmochim. Acta 51 (3), 567–587. https://doi.org/10.1016/0016-7037(87)90070-6.

Brimhall, G.H., Chadwick, O.A., Lewis, C.J., Compston, W., Williams, I.S., Danti, K.J., Dietrich, W.E., Power, M.E., Hendricks, D., Bratt, J., 1992. Deformational mass transport and invasive processes in soil evolution. Science 255 (5045), 695–702.

Brown, G., 1980. Associated minerals. In: Brindley, G.W., Brown, G. (Eds.), Crystal Structures of Clay Minerals and Their X-Ray Identification, Monograph 5. Mineralogical Society, London, pp. 361–410.

Bulmer, C.E., 1992. Pedogenesis of soils derived from ultramafic rocks and tephra in southwestern British Columbia. Department of Soil Science. University of British Columbia.

Bulmer, C.E., Lavkulich, L.M., 1994. Pedogenic and geochemical processes of ultramafic soils along a climatic gradient in southwestern British Columbia. Can. J. Soil Sci. 74, 165–177. https://doi.org/10.4141/cjss94-024.

Burt, R., 2004. Soil Survey Laboratory Methods Manual. Soil Survey Investigations Report No. 42. Version 4.0. Natural Resources Conservation Service, National Soil Survey Center, Lincoln, NE.

Buurman, P., Meijer, E.L., van Wikck, J.H., 1988. Weathering of chlorite and vermiculite in ultramafic rocks of Cabo Ortegal, Northwestern Spain. Clays Clay Miner. 36 (3), 263–269. https://doi.org/10.1346/CCMN.1988.0360308.

Caillaud, J., Proust, D., Righi, D., Martin, F., 2004. Fe-rich clays in a weathering profile developed from serpentinite. Clays Clay Miner. 52, 779–791. https://doi.org/10.1346/CCMN.2004.05206013.

Caillaud, J., Proust, D., Righi, D., 2006. Weathering sequences of rock-forming minerals in a serpentinite: influence of microsystems on clay mineralogy. Clays Clay Miner. 54 (1), 87–100. https://doi.org/10.1346/CCMN.2006.0540111.

Caillaud, J., Proust, D., Philippe, S., Fontain, C., Fialin, M., 2009. Trace metals distribution from a serpentinite weathering at the scales of the weathering profile and its related weathering microsystems and clay minerals. Geoderma 149 (3–4), 199–208. https://doi.org/10.1016/j.geoderma.2008.11.031.

Carnicelli, S., Mirabella, A., Cecchini, G., Sanesi, G., 1997. Weathering of chlorite to a low-charge expandable mineral in a Spodosol on the Appennines Mountains. Italy. Clays Clay Miner. 45 (1), 28–41. https://doi.org/10.1346/CCMN.1997.0450104.

Chadwick, O.A., Brimhall, G.H., Hendricks, D.M., 1990. From a black to a gray box – a mass balance interpretation of pedogenesis. Geomorphol 3, 369–390. https://doi.org/10.1016/0169-555X(90)90012-F.

Cleaves, E.T., Fisher, D.W., Bricker, O.P., 1974. Chemical weathering of serpentinite in the Eastern Piedmont of Maryland. Geol. Soc. Am. Bull. 85, 437–444. https://doi.org/10.1130/0016-7606(1974)85%3C437:CWOSIT%3E2.0.CO;2.

D'Amico, M.E., Julitta, F., Previtali, F., Cantelli, D., 2008. Podzolization over ophiolitic materials in the western Alps (Natural Park of Mont Avic, Aosta Valley, Italy). Geoderma 146, 129–136. https://doi.org/10.1016/j.geoderma.2008.05.025.

D'Amico, M.E., Calabrese, F., Rossetti, A., Previtali, F., 2009. Heavy metals and biological properties of subalpine soils on ophiolites in the Italian Western Alps. Northeast. Natural. 16 (sp5), 193–214. https://doi.org/10.1656/045.016.0516.

D'Amico, M.E., Bonifacio, E., Zanini, E., 2014. Relationships between serpentine soils and vegetation in a xeric inner-Alpine environment. Plant and Soil 376, 111–128. https://doi.org/10.1007/s11104-013-1971-y.

D'Amico, M., Almeida, J.P., Barbieri, S., Castelli, F., Sgura, E., Sineo, G., Martin, M., Bonifacio, E., Wallander, H., Celi, L., 2020. Ectomycorrhizal utilization of different phosphorus sources in a glacier forefront in the Italian Alps. Plant and Soil 446, 81–95. https://doi.org/10.1007/s11104-019-04342-0.

D'Amico, M.E., Casati, E., El Khair, D.A., Cavallo, A., Barcella, M., Previtali, F., 2023. Aeolian inputs and dolostone dissolution involved in soil formation in Alpine karst landscapes (Corna Bianca, Italian Alps). Catena 230, 107254. https://doi.org/10.1016/j.catena.2023.107254.

Dal Piaz, G., Gianotti, F., Monopoli, B., Pennacchioni, G., Tartarotti, P., Schiavo, A., Carraro, F., Bistacchi, A.L.P., Massironi, M., Martin, S. Ratto, S., 2011. Note Illustrative della CARTA GEOLOGICA D'ITALIA alla scala 1: 50.000: foglio 091CHATILLON.

De Caritat, P., Hutcheon, I., Walshey, J.L., 1993. Chlorite geothermometry: a review. Clays Clay Min. 41 (2), 219–239. https://doi.org/10.1346/CCMN.1993.0410210.

Di Mauro, B., Garzonio, R., Rossini, M., Filippa, G., Pogliotti, P., Galvagno, M., Morra di Cella, U., Migliavacca, M., Baccolo, G., Clemenza, M., Delmonte, B., 2019. Saharan dust events in the European Alps: role in snowmelt and geochemical characterization. Cryosph 13 (4), 1147–1165. https://doi.org/10.5194/tc-13-1147-2019.

Dixon, J.B., 1989. Kaolin and serpentine group minerals. In: Dixon, J.B., Weed, S.B. (Eds.), Minerals in Soil Environments. Soil Science Society of America, Madison, pp. 467–526.

Ducloux, J., Meunier, A., Velde, B., 1976. Smectite, vermiculite and a regular interlayered chlorite-vermiculite in soils developed on a small serpentinite body, Massif Central. France. Clay Miner. 11, 121–135. https://doi.org/10.1180/claymin.1976.011.2.04.

Eger, A., Almond, P.C., Condron, L.M., 2011. Pedogenesis, soil mass balance, phosphorus dynamics and vegetation communities across a Holocene soil chronosequence in a super-humid climate, South Westland. New Zealand. Geoderma 163 (3–4), 185–196.

Egli, M., Fitze, P., 2000. Formulation of pedologic mass balance based on immobile elements: a revision. Soil Sci. 165 (5), 437–443.

Egli, M., Mirabella, A., Fitze, P., 2001a. Clay mineral formation in soils of two different chronosequences in the Swiss Alps. Geoderma 104 (1), 144–175. https://doi.org/10.1016/S0016-7061(01)00079-9.

Egli, M., Fitze, P., Mirabella, A., 2001b. Weathering and evolution of soils formed on granitic, glacial deposits: results from chronosequences of swiss alpine environments. Catena 45 (1), 19–47. https://doi.org/10.1016/S0341-8162(01)00138-2.

Egli, M., Mirabella, A., Sartori, G., Zanelli, R., Bischof, S., 2006. Effect of north and south exposure on weathering rates and clay mineral formation in Alpine soils. Catena 67, 155–174. https://doi.org/10.1016/j.catena.2006.02.010.

Egli, M., Mirabella, A., Sartori, G., Giaccai, D., Zanelli, R., Plotze, M., 2007. Effect of slope aspect on transformation of clay minerals in Alpine soils. Clay Min. 42 (3), 373–398. https://doi.org/10.1180/claymin.2007.042.3.09.

Egli, M., Mirabella, A., Sartori, G., 2008. The role of climate and vegetation in weathering and clay mineral formation in late quaternary soils of the swiss and Italian Alps. Geomorphol 102 (3–4), 307–324. https://doi.org/10.1016/j.geomorph.2008.04.001.

Fisher, H., Luster, J., Gehring, A.U., 2008. Magnetite weathering in a Vertisol with seasonal redox-dynamics. Geoderma 143, 41–48. https://doi.org/10.1016/j.geoderma.2007.10.004.

Finsinger, W., Lane, C.S., van Den Brand, G.J., Wagner-Cremer, F., Blockley, S.P.E., Lotter, A.F., 2011. The Lateglacial Quercus expansion in the southern European Alps: rapid vegetation response to a late Allerød climate warming? J. Quat. Sci. 26 (7), 694–702. https://doi.org/10.1002/jqs.1493.

Freyssinet, P., Farah, A.S., 2000. Geochemical mass balance and weathering rates of ultramafic schists in Amazonia. Chem. Geol. 170 (1–4), 133–151. https://doi.org/10.1016/S0009-2541(99)00245-4.

Garnier, J., Quantin, C., Guimaraes, E., Garg, V.K., Martins, E.S., Becquer, T., 2009. Understanding the genesis of ultramafic soils and catena dynamics in Niquelandia, Brazil. Geoderma 151, 204–241. https://doi.org/10.1016/j.geoderma.2009.04.020.

Gasser, U.G., Juchler, S.J., Hobson, W.A., Sticher, H., 1994. The fate of chromium and nickel in subalpine soils derived from serpentinite. Can. J. Soil Sci. 75, 187–195. https://doi.org/10.4141/cjss95-026.

Gild, C., Geitner, C., Sanders, D., 2018. Discovery of a landscape-wide drape of late-glacial aeolian silt in the western Northern Calcareous Alps (Austria): first results and implications. Geomorphology 301, 39–52. https://doi.org/10.1016/j.geomorph.2017.10.025.

Goudie, A.S., Middleton, N.J., 2001. Saharan dust storms: nature and consequences. Earth Sci. Rev. 56 (1–4), 179–204. https://doi.org/10.1016/S0012-8252(01)00067-8.

Guerzoni, S., Molinaroli, E., Chester, R., 1997. Saharan dust inputs to the western Mediterranean Sea: depositional patterns, geochemistry and sedimentological implications. Deep Sea Res. Part II: Topical Studies. Oceanography 44 (3–4), 631–654. https://doi.org/10.1016/S0967-0645(96)00096-3.

Herbillon, A.J., Makumbi, M.N., 1975. Weathering of chlorite in a soil derived from a chloriteschist under humid tropical conditions. Geoderma 13, 89–104. https://doi.org/10.1016/0016-7061(75)90059-2.

Karathanasis, A.D., Hajek, B.F., 1983. Transformation of smectite to kaolinite in naturally acid soil systems: structural and thermodinamic considerations. Soil Sci. Soc. Am. J. 47, 158–163. https://doi.org/10.2136/sssaj1983.03615995004700010031x.

Kierczak, J., Neel, C., Bril, H., Puziewics, J., 2007. Effect of mineralogy and pedoclimatic variations on Ni and Cr distribution in serpentine soils under temperate climate. Geoderma 142, 165–177. https://doi.org/10.1016/j.geoderma.2007.08.009.

Kierczak, J., Pietranik, A., Pędziwiatr, A., 2021. Ultramafic geoecosystems as a natural source of Ni, Cr, and Co to the environment: a review. Sci. Tot. Env. 755, 142620. https://doi.org/10.1016/j.scitotenv.2020.142620.

Kowalska, J.B., Gąsiorek, M., Zadrożny, P., Nicia, P., Waroszewski, J., 2021. Deep subsoil storage of trace elements and pollution assessment in mountain Podzols (Tatra Mts., Poland). Forests 12 (3), 291. https://doi.org/10.3390/f12030291.

Kröpelin, S., Verschuren, D., Lézine, A.M., Eggermont, H., Cocquyt, C., Francus, P., Cazet, J.P., Fagot, M., Rumes, B., Russell, J.M., Darius, F., 2008. Climate-driven ecosystem succession in the Sahara: the past 6000 years. Science 320 (5877), 765–768. https://doi.org/10.1126/science.1154913.

Küfmann, C., 2003. Soil types and eolian dust in high-mountainous karst of the Northern Calcareous Alps (Zugspitzplatt, Wetterstein Mountains, Germany). Catena 53, 211–227. https://doi.org/10.1016/S0341-8162(03)00075-4.

Lawrence, C.R., Reynolds, R.L., Ketterer, M.E., Neff, J.C., 2013. Aeolian controls of soil geochemistry and weathering fluxes in high-elevation ecosystems of the Rocky Mountains. Colorado. Geochim. Cosmochim. Acta 107, 27–46. https://doi.org/10.1016/j.gca.2012.12.023.

Lee, B.D., Sears, S.K., Graham, R.C., Amrhein, C., Vali, H., 2003. Secondary mineral genesis from chlorite and serpentine in an ultramafic soil toposequence. Soils Sci. Soc. Am. J. 67, 1309–1317. https://doi.org/10.2136/sssaj2003.1309.

Lessovaia, S.N., Goryachkin S., Polekhovsky Y., Ershova V., Filimonov A., 2016a. Abiotic and Biotic Processes of Mineral Weathering in Tundra Soils on Ultramafic and Mafic Rocks of the Polar Urals, Russia. In: Frank-Kamenetskaya et al. (Eds.): Biogenic—Abiogenic Interactions in Natural and Anthropogenic Systems. Lecture Notes in Earth System Sciences, Springer.

Lessovaia, S.N., Dultz, S., Plötze, M., Andreeva, N., Polekhovsky, Y., Filimonov, A., Momotova, O., 2016b. Soil development on basic and ultrabasic rocks in cold environments of Russia traced by mineralogical composition and pore space characteristics. Catena 137, 596–604. https://doi.org/10.1016/j.catena.2014.11.020.

Lin, F.C., Clemency, C.V., 1981. The dissolution kinetics of brucite, antigorite, talc and phlogopite at room temperature and pressure. Am. Min. 66, 801–806.

Lindsay, W.L., 1979. Chemical equilibria in soils. John Wiley & Sons, New York.

Manceau, A., Calas, G., Decarreau, A., 1985. Nickel-bearing clay minerals: I. Optical spectroscopic study of nickel crystal chemistry. Clay Min. 20 (3), 367–387. https://doi.org/10.1180/claymin.1985.020.3.08.

Mercalli, L., Cat Berro, D., 2003. Atlante Climatico Della Valle d'Aosta. Torino, Italy; Vol, SMS, p. 2.

Mirabella, A., Egli, M., 2003. Structural transformation of clay minerals in soils of a climosequence in an Italian alpine environment. Clays Clay Min. 51, 264–278. https://doi.org/10.1346/CCMN.2003.0510303.

Moore, J.C.V., Reynolds, R.C., 1997. X-Ray Diffraction and the Identification and Analysis of Clay Minerals. Oxford University Press, Oxford, New York.

Moreno, T., Querol, X., Castillo, S., Alastuey, A., Cuevas, E., Herrmann, L., Mounkaila, M., Elvira, J., Gibbons, W., 2006. Geochemical variations in aeolian mineral particles from the Sahara–Sahel Dust Corridor. Chemosphere 65 (2), 261–270. https://doi.org/10.1016/j.chemosphere.2006.02.052.

Munroe, J.S., Santis, A.A., Soderstrom, E.J., Tappa, M.J., Bauer, A.M., 2024. Mineral dust and pedogenesis in the alpine critical zone. Soil 10 (1), 167–187. https://doi.org/10.5194/soil-10-167-2024.

Musielok, Ł., Buczek, K., Karcz, T., 2022. Relief-induced feedback mechanisms controlling local podzolization occurrence on flysch slopes–examples from outer Western Carpathians (southern Poland). Catena 213, 106124. https://doi.org/10.1016/j.catena.2022.106124.

Musso, A., Lamorski, K., Sławiński, C., Geitner, C., Hunt, A., Greinwald, K., Egli, M., 2019. Evolution of soil pores and their characteristics in a siliceous and calcareous proglacial area. Catena 182, 04154. https://doi.org/10.1016/j.catena.2019.104154.

Nahon, D.B., Paquet, H., Delvigne, J., 1988. Lateritic weathering of ultramafic rocks and the concentration of nickel in the western Ivory Coast. Econ. Geol. 77 (5), 1159–1175. https://doi.org/10.2113/gsecongeo.77.5.1159.

Noack, Y., Colin, F., 1986. Chlorites and chloritic mixed-layer minerals in profiles on ultrabasic rocks from Moyango (Ivory Coast) and Angiquinho (Brazil). Clay Min. 21, 171–182. https://doi.org/10.1180/claymin.1986.021.2.06.

Parfitt, R.L., Henmi, T., 1982. Comparison of an oxalate extraction method and an infrared spectroscopic method for determine allophane in soil clays. Soil Sci. Plant Nutr. 28, 183–190. https://doi.org/10.1080/00380768.1982.10432435.

Pavan, C., Celi, L., D'Amico, M.E., Freppaz, M., Siniscalco, C., Zaccone, C., 2016. Relazione tra specie vegetali e clima nella formazione di una torbiera alpina su serpentinte. Nimbus 75.

Pilar, M.R., Roveda, L.F., Lima, M.R., de Oliveira Junior, J.C., 2024. Organic carbon and short-range order minerals responsible for cementation of the spodic horizon (ortstein): a new proposal of chemical extractions in undisturbed samples. Soil Res. 62 (4). https://doi.org/10.1071/SR24034.

Porder, S., Hilley, G.E., Chadwick, O.A., 2007. Chemical weathering, mass loss, and dust inputs across a climate by time matrix in the hawaiian Islands. Earth Planet. Sci. Lett. 258 (3–4), 414–427. https://doi.org/10.1016/j.epsl.2007.03.047.

Post, J.L., Borer, L., 2000. High-resolution infrared spectra, physical properties and micromorphology of serpentines. Appl. Clay Sci. 16, 73–85. https://doi.org/10.1016/S0169-1317(99)00047-2.

Rabenhorst, M.C., Foss, J.E., Fanning, D.S., 1982. Genesis of Maryland soils formed from serpentinite. Soil Sci. Soc. Am. J. 46, 607–616. https://doi.org/10.2136/sssaj1982.03615995004600030032x.

Räisänen, M.L., Kashulina, G., Bogatyrev, I., 1997. Mobility and retention of heavy metals, arsenic and sulphur in podzols at eight locations in northern Finland and Norway and the western half of the Russian Kola Peninsula. J. Geochem. Expl. 59 (3), 175–195. https://doi.org/10.1016/S0375-6742(97)00014-9.

Rodriguez-Navarro, C., di Lorenzo, F., Elert, K., 2018. Mineralogy and physicochemical features of Saharan dust wet deposited in the Iberian Peninsula during an extreme red rain event. Atm. Chem. Phys. Disc. 18 (13), 10089–10122. https://doi.org/10.5194/acp-18-10089-2018.

Sasaki, S., Matsuno, T., Kondo, Y., 1968. A podsol derived from serpentine rocks in Hokkaido. Japan. Soil Sci. Plant Nutr. 14, 99–109. https://doi.org/10.1080/00380768.1968.10432752.

Scheuvens, D., Schütz, L., Kandler, K., Ebert, M., Weinbruch, S., 2013. Bulk composition of northern african dust and its source sediments—A compilation. Earth Sci. Rev. 116, 170–194. https://doi.org/10.1016/j.earscirev.2012.08.005.

Schreier, H., Omueti, J.A., Lavkulich, L.M., 1987. Weathering processes of asbestos-rich serpentinic sediments. Soil Sci. Soc. Am. J. 51, 993–999. https://doi.org/10.2136/sssaj1987.03615995005100040032x.

Senkayi, A.L., Dixon, J.B., Hossner, L.R., 1981. Transformation of chlorite to smectite through regularly interstratified intermediates. Sol. Sci. Soc. Am. J. 45, 650–656. https://doi.org/10.2136/sssaj1981.03615995004500030043x.

Serra, E., Valla, P.G., Gribenski, N., Guedes Magrani, F., Carcaillet, J., Delaloye, R., Grobéty, B., Braillard, L., 2021. Geomorphic response to the lateglacial–holocene transition in high alpine regions (Sanetsch pass, swiss alps). Boreas 50 (1), 242–261. https://doi.org/10.1111/bor.12480.

Spinola, D., Portes, R., Fedenko, J., Lybrand, R., Dere, A., Biles, F., Trainor, T., Bowden, M.E., D'Amore, D., 2022. Lithological controls on soil geochemistry and clay mineralogy across Spodosols in the coastal temperate rainforest of southeast Alaska. Geoderma 428, 116211. https://doi.org/10.1016/j.geoderma.2022.116211.

Stuut, J.B., Smalley, I., O'Hara-Dhand, K., 2009. Aeolian dust in Europe: african sources and European deposits. Quat. Int. 198 (1–2), 234–245. https://doi.org/10.1016/j.quaint.2008.10.007.

Styllas, M., Pennos, C., Persoiu, A., Godelitsas, A., Papadopoulou, L., Aidona, E., Kantiranis, N., Ducea, M.N., Ghilardi, M., Demory, F., 2023. Aeolian dust accretion outpaces erosion in the formation of Mediterranean alpine soils. New evidence from the periglacial zone of Mount Olympus. Greece. Earth Surf. Proc. Landforms 48 (14), 3003–3021. https://doi.org/10.1002/esp.5669.

Thorez, J., 1975. Phyllosilicates and Clay Minerals. Lelotte, Dison, Belgium.

Ugolini, F.C., Minden, R., Dawson, H., Zacgara, J., 1977. An example of soil process in the *Abies amabilis* zone of the central Cascades, Washington. Soil Sci. 124, 291–302.

van Breemen, N., Lundström, U.S., Jongmans, A.G., 2000. Do plants drive podzolization via rock-eating mycorrhizal fungi? Geoderma 94 (2–4), 163–171. https://doi.org/10.1016/S0016-7061(99)00050-6.

Van Mourik, J.M., de Vet, S.J., 2015. Iron stocks of buried Podzols: Endogenic iron deficits and potential exogenic enrichment in the Maashorst region, SE Netherlands. Catena 132, 97–104. https://doi.org/10.1016/j.catena.2015.01.019.

Varga, G., Cserháti, C., Kovács, J., Szalai, Z., 2016. Saharan dust deposition in the Carpathian Basin and its possible effects on interglacial soil formation. Aeol. Res. 22, 1–12. https://doi.org/10.1016/j.aeolia.2016.05.004.

Wilson, M.J., 1987. X-ray powder diffraction methods. In: Wilson, M.J. (Ed.), A Handbook of Determinative Methods in Clay Mineralogy. Blackie and Son Ltd., Glasgow, GB, pp. 26–98.